SQUIDs in Nondestructive Evaluation

Hans-Joachim Krause, PGI-8, Forschungszentrum Jülich, Germany
Michael Mück, ez SQUID Mess- und Analysegeräte, Sinn, Germany
Saburo Tanaka, Toyohashi University of Technology, Toyohashi, Japan

Introduction

A growing use of SQUIDs is in the detection of defects, such as cracks, inclusions, or holes, in a variety of materials and structures. Ideally, the material tested for such defects should not be destroyed by the detection process, hence the term nondestructive testing (NDT), or nondestructive evaluation (NDE). SQUIDs have been used for nondestructive evaluation of various materials since the 1980s. Among the first experiments on SQUID NDE were the remote detection of surface breaking cracks in ferromagnetic steel by Bain *et al.* [1], plastic deformation in magnetic steels by Evanson *et al.* [2], Barkhausen jumps in iron samples by Weinstock *et al.* [3] and the location of metal pipelines by Weinstock *et al.* [4]. Capobianco *et al.* [5] carried out eddy-current-testing experiments at the National Bureau of Standards. In other work, Bellingham *et al.* [6] studied electrolytic corrosion processes in non-voltaic cells, and Hibbs *et al.* [7] measured corrosion currents with a SQUID array. Wunderlich *et al.* [8] studied the field gradient distribution of hardened steel cylinders with a HTS SQUID to detect mechanical stress in such cylinders. Weinstock *et al.* [9] tested NbTi/Cu wires for defects using an HTS dc SQUID. A field which has been widely explored is nondestructive testing of aircraft parts using eddy current techniques, for example, by Wikswo [10], Hohmann *et al.* [11], Kreutzbruck *et al.* [12], Ruosi *et al.* [13], and Tavrin *et al.* [14]. Finally, prestressed concrete bridge structures have been tested by Krause *et al.* [15] making dc measurements of the remanent magnetization of the steel reinforcement with a portable HTS SQUID.

We will discuss in this Chapter the basic principles of nondestructive evaluation using SQUIDs in static and in alternating magnetic fields. For each field, we will present a brief review of work done, and then discuss one example in more detail, to familiarize the reader with the topic. For further work, we refer the reader to the references listed at the end of this Chapter, and to Volume II of the SQUID handbook [16].

NDE in static magnetic fields

The first experiments on SQUID NDE used static magnetic fields to enhance changes in the magnetic field produced by defects in the material under test. The basic testing configuration is outlined in Fig. 1. A permanent magnet produces a large static field, which will polarize the sample. The sample then is passed below the SQUID; any change in the magnetic susceptibility of the sample will produce a change in the magnetic field measured by the SQUID. The information thus gained by this experiment is about a variation in the susceptibility of the sample. Defects, which have a susceptibility different from that of the surrounding material can be detected, provided that the change in magnetic field produced by the variation in susceptibility is larger than the noise of the SQUID, and any environmental noise. As static fields have to be detected, and environmental magnetic noise has a large 1/f component, the testing has usually to be done in a magnetically shielded environment. If the samples under test are small, a small mu-metal box will be sufficient to suppress environmental noise.

Donaldson *et al.* [1,2] were the first to use this approach to detect flaws in ferric steel plates. They were able to find small slots in such plates with distances between the slot and SQUID of up to 10 cm. In other work, Wikswo *et al.* [17] could detect flaws and voids even in nonmagnetic materials, such as plexiglass. Tavrin *et al.* [14] detected magnetic inclusions in turbine discs made from nonmagnetic alloys, using a HTS SQUID with a sensitivity of about 130 $fT/Hz^{1/2}$. They could reliably detect defects with masses m ~ 1mg in a depth of up to 70 mm; at a depth of 4 mm, even defects with m ~ 10 µg could be found. Finally, Bonavolontà *et al.* [18] detected mechanical fatigue in structural steel using a SQUID.

A number of groups [19-25] applied this technique to the detection of ferromagnetic inclusions in various materials. For example, Tanaka *et al.* [19, 20, 23-25] describe a system which is used to detect magnetic contaminants in (canned) food products and active-material coated foils for Li-ion batteries. Examples of these contaminants in both, metallic foils as well as food, are small metal chips from raw materials or the processing machinery. The current requirements for commercial applications, such as Li-ion batteries, are to find metallic particles that have a diameter greater than 50 µm. However, particles smaller than about 100 µm cannot be detected by X-ray imaging, which is commonly used as the inspection method. For this reason, Tanaka *et al.* developed a highly sensitive detection system for small contaminant particles based on a high-temperature-superconductor (HTS) SQUID. They use a planar gradiometer and a horizontal magnetization of the sample prior to measurement.

The principle of detecting magnetic contaminants with their system is shown in Fig. 2. A permanent magnet horizontally magnetizes the metallic contaminants and the test object itself. The sheet material, or food, to be tested is passed through a ring-shaped permanent magnet with a flux density of 1.3 T. The remanent magnetic flux from a possible metallic contaminant in the sheet is then detected by a number of SQUID gradiometers as the sheet passes below these sensors. Sheets with a maximum width of 100 mm can be tested with a maximum speed of 100 m/min. The detection unit including the shield and the cryostat is mechanically well isolated from the magnet and the driving components, in order to protect them from mechanical vibrations. The dimensions (length × width × height) of the entire system are 2200 mm × 700 mm × 1380 mm. For food contaminant detection, the requirement for the detection size is greater than 0.5 mm in diameter. A major Japanese dairy company introduced and equipped a high Tc SQUIDs detection system [19, 25] in 2005; this system is still in use every day in the factory

The liquid nitrogen (LN_2) cryostat used for maintaining the temperature of the eight SQUID gradiometers at 77 K is custom designed. The outer jacket of the cryostat is fabricated from aluminum alloy, and the LN_2 tank is made from copper. The total volume of LN_2 is 1.1 ℓ, which is sufficient for 14-h operation without refilling. In order to achieve a small standoff-distance between the SQUIDs and the sample under test, the SQUIDs are placed inside the insulation vacuum of the dewar, rather than immersed in the LN_2. To thermally anchor the SQUIDs to the LN_2 bath, they are mounted to eight sapphire rods protruding through the bottom of the LN_2 container into the insulation vacuum. In this configuration, the sample under test can be placed as close as 1–2 mm to the SQUIDs [26]. The dewar containing the SQUIDs is placed inside a small magnetic shield to suppress external magnetic fields. This shield measures 630 mm × 480 mm × 704 mm, and is made from 2-mm thick mu-metal. The measured shielding factors (*SF*) of the magnetically shielded box for each direction at 1 Hz are SF_x = 50,000, SF_y = 33,000, and SF_z = 25,000. These factors are sufficient for operation in a typical laboratory or industrial environment.

The white noise level of the SQUID gradiometers employed is 20–30 $\mu\phi_0/Hz^{1/2}$ at 100 Hz. These values are 10 $\mu\phi_0/Hz^{1/2}$ higher than the values measured when the SQUIDs are immersed in LN_2 because of the relatively high temperature of the sapphire rods (T > 77K). The base-line lengths of the gradiometers are 3 mm. Three SQUID loops are directly connected to a differential pickup loop consisting of rectangular pickup loops (3 mm × 8 mm for each loop). For data post-processing, the signal is passed through a high-pass filter with a cutoff frequency of 0.5 Hz, and a second-order low-pass filter with a cutoff frequency of 100 Hz.

Small iron (S50C) balls with a diameter of 35–82 μm are used to characterize the system. The balls are first magnetized by the permanent magnet, and their remanent field is measured with the SQUID gradiometers. Real-time traces of the gradiometer output and the peak-to-peak values as a function of the ball diameter are shown in Fig. 3 (left). Even the smallest balls produce a typical gradiometric signature with a high signal-to-noise ratio. The peak-to-peak values roughly scale with the cube of the diameter, specifically $D^{2.6}$ (see Fig. 3, right), which Tanaka *et al.* believe can be attributed to the anisotropy of the magnetization of the balls.

Yet another nondestructive evaluation scheme using static magnetic fields is the so-called Magnetic Flux Leakage (MFL) technique [27]. This scheme is well suited for the inspection of prestressed steel tendons in concrete beams or bridge decks [27-29]. Tendon ruptures may occur when water penetrates the duct due to inadequate grouting. Hydrogen-induced corrosion of the steel tendons may then be initiated, which will eventually cause cracks of single strands and could finally lead to a collapse of the entire structure. The basic principle of MFL is as follows. Tendons hidden in the concrete are magnetized by a static magnetic field applied from outside the concrete by means of a yoke magnet. The tendon can be considered as a high-permeability magnetic field guide. Ruptures or reductions of its cross-section produce a resulting magnetic leakage flux as they act as local disturbances in the flux guide. The ensuing magnetic stray field is then recorded. To this end, a probe containing the magnetization device (yoke magnet) and the magnetic field sensors is moved along the direction of the prestressed tendon on the concrete surface (see Fig. 4).

Krause *et al.* [15, 30] employed this technique to evaluate tendons inside highway bridges. They used four high-T_c dc SQUID magnetometers with ramp junctions optimized for high-field performance [31] to detect the magnetic stray field in the center of the yoke. The magnetic field was recorded while the exciting field was applied (active stray field measurement) and again after the magnet had been switched off (remanent field measurement). They could show that a single cracked rebar can be found in post-tensioned members, even though the magnetic signature of the crack is attenuated significantly by the shielding effect of the surrounding flawless tendons and the duct around the strands. Fig. 5 shows a result of a SQUID measurement on a German highway bridge. At each location, nine scans of 260 cm length were conducted at different premagnetization states. Before each measurement scan, the SQUID sensors were heated just above the critical temperature of the superconducting film in order to eliminate trapped magnetic flux. Details on the signal analysis procedure were given in Ref. [29]. Fig. 5 shows the correlation coefficient and the crack signal amplitude of the evaluated stray field and remanent field scans at a selected location of the bridge. The indication at x = 82 ± 5 cm, gave a correlation coefficient and a rupture signal amplitude well above the threshold. Opening the bridge deck confirmed that two of the eight rebar wires were cracked at this location.

Eddy current testing

Eddy current testing is a well-established procedure to test electrically-conducting objects for defects. In this procedure, one produces an ac-magnetic field, which in turn induces eddy currents in the sample under test. If the object has homogeneous conductivity, i.e., no defects are present, the local eddy current density will be homogeneous as well. Defects will locally change the conductivity and thus lead to a distortion of the eddy current flow in the vicinity of the defect (see Fig. 6, left).

Defects can obviously be localized by measuring the local eddy current density. As a direct measurement of the eddy currents is difficult, one rather measures the magnetic field produced by the eddy currents directly above the sample. In a conventional eddy current test set, the magnetic field produced by the eddy currents (sometimes called the secondary field to distinguish it from the primary field, which is used to induce the eddy currents) is measured with an induction coil (shown in Fig. 6 left). The penetration depth (skin depth) δ of eddy currents in the sample is a function of the conductivity of the object, its permeability and the frequency of the eddy currents. The skin depth $\delta = (\omega\sigma\mu\mu_0)^{-1/2}$, where ω is the eddy current frequency, σ the conductivity of the object, μ the magnetic permeability and $\mu_0 = 4\pi\times10^{-7}$ H/m the magnetic permeability of vacuum. Electrically well conducting materials, such as copper ($\sigma = 6.25\times10^{7}$ A/Vm), thus require the excitation of eddy currents with much lower frequency than, for example, indium-tin oxide (ITO, $\sigma \approx 1\times10^{5}$ A/Vm), to produce a substantial eddy current flow in a certain depth inside the material.

In the case of conventional eddy current testing, the sensitivity for finding defects scales as $1/\omega$, as the field sensitivity of an induction coil is proportional to ω. The typical field noise of an induction coil used as field sensor in conventional eddy current equipment is about 1 nT/$\sqrt{\text{Hz}}$ at eddy current frequencies of about 100 kHz, or about 1 μT/$\sqrt{\text{Hz}}$ at 100 Hz. Surprisingly enough, even the rather poor sensitivity at low frequencies is sufficient to find defects. However, some applications require a much higher field sensitivity, especially at low excitation frequencies. For example, certain aircraft parts, such as layered stacks of aluminum sheets or aircraft wheels, are made from relatively thick aluminum. In order to achieve sufficient eddy current density deep inside these materials, a relatively low eddy current frequency must be used (e.g., 400 Hz for a flaw in aluminum in a 15-mm depth). The high field sensitivity of SQUIDs at low frequencies makes it ideally suited for the evaluation of such relatively thick conductive objects.

There are several ways to induce electric currents in the sample to be tested. A dc or ac current can simply be induced by connecting the sample with two wires to a power supply. This so-called direct current injection has several disadvantages: wires have to be attached to the sample, which —depending on the shape of the sample— might be difficult. It might also be difficult to determine the actual current distribution, and the obtainable current density might be low in case of a large-area sample. The signals, which potential defects might produce, will be only small for low current densities.

In contrast to direct injection of dc or ac currents into the sample, the induction of eddy currents by an external coil (usually called excitation coil) generates a spatially well-confined current distribution. As no electrical connections to the sample are required, eddy current NDE is more practical to use than direct current injection. Also, by choosing an appropriate coil geometry, the current density at potential defects can be made much higher. However, the choice of the optimum measurement parameters, such as the excitation frequency, is more critical. Furthermore, calculation of the current distribution in the sample from the measured field distribution tends to be more difficult than in the case of direct current injection. As usually users of NDE systems are not much interested in the current flow in the sample, but rather want to find defects, this is not a big disadvantage.

In order to minimize the excitation field at the location of the SQUID, a gradiometric excitation coil (a so-called double-D coil, see, e.g., [11-13]) can be used. By carefully moving this coil below the SQUID to find its optimum position, the cross talk between excitation coil and SQUID can be kept lower than 0.1%. Alternatively, the magnetic field of a circular excitation coil can be compensated electronically at the location of the SQUID by passing part of the excitation current in the modulation coil used for flux locking the SQUID. By carefully adjusting the amplitude and phase of the compensation current, the excitation field at the SQUID can be reduced by a factor of up to 1000. An even higher compensation factor is, in principle, possible, but drift then requires a frequent readjustment of amplitude and phase of the compensation current. As the obtainable signal-to-noise ratio is directly proportional to the amplitude of the excitation field, the latter should be as large as possible. Field amplitudes of mT should be aimed at.

A number of groups have studied eddy-current testing procedures with a (in most cases HTS) SQUID [see, e.g. 10-13]. The main interest here was in testing aircraft parts. Besides conventionally used aluminum and titanium alloys, carbon-fibre reinforced plastics were investigated, e.g., by Ruosi et al. [32], Graham et al. [33], and Bonavolontà *et al.* [34, 35]. Such polymers have become increasingly popular in aircrafts because of their high specific stiffness and high specific strength.

Welzel *et al.* [36] studied a LTS SQUID-based eddy-current NDE system to test flat niobium sheets used to make superconducting resonators for particle accelerators. Such niobium sheets (usually of size 300 × 300 mm^2) have to be tested for small inclusions of foreign materials, such as tantalum, as these deteriorate the quality factor of the superconducting resonator made from such sheets. The requirements here are the detection of tantalum inclusions having a volume of as small as 10^{-12} m^3 in a short time; the time needed to test a 30×30 cm^2 sheet should not be longer than a few minutes, to be able to test a large number of sheets in an acceptable time. We discuss this system in some detail, as it gives a good example of a highly-sensitive SQUID eddy-current NDE system.

Fig. 6 (right) shows the principle of eddy current testing of a niobium sheet. A circular coil, usually with a diameter of a few mm, generates eddy currents in the niobium sheet. Inhomogeneities, such as cracks or inclusions of materials having a conductivity different from that of niobium, lead to a distortion of the eddy current flow, and thus to a change in the eddy current field, which is detected by scanning the sheet with a niobium SQUID. As a high spatial resolution is usually required, a circular excitation coil with diameter ~ 2 mm was used instead of the usual double-D coil; the excitation field at the SQUID was reduced by electronic compensation. In this example, the excitation field was of up to 1 mT peak-to-peak; the required excitation current was about 2 A peak-to-peak. Dissipation in the excitation coil raised its temperature to about 60°C in this case. Finally, the SQUID was cooled in a low-noise fiberglass helium dewar for biomagnetic measurements, permitting a small stand-off distance between SQUID and sample of about 6 mm.

The optimum excitation frequency is given by the skin depth in the material under test and the expected depth of the inclusions. In a superconducting resonator, rf currents will only flow at the surface of the resonator, so in principle one would only need to find defects in a depth of a few μm. However, during fabrication of the resonator, up to 0.5 mm of niobium are etched away from the surface, so that even defects in this depth might lead to a reduction in the obtainable resonator quality factor. In order to maximize the eddy-current density in a 0.5 mm thick layer at the surface of the sheet, an excitation frequency of about 40 kHz would be required. Although the excitation field at the location of the SQUID is minimized by the compensation coil, a dynamic range of about 20 to 50 flux quanta is still needed at this frequency to prevent unlocking of the flux-locked loop by scanning across the edges of the sheet. The slew rate required of the flux-locked loop then is about 4 to 10 $\Phi_0/\mu s$, which can easily obtained with a conventional ac flux-modulated flux-locked loop with a modulation frequency of 4 MHz; a dynamic range of about 15 flux quanta at 100 kHz is possible.

Welzel *et al.* [36] used a niobium dc SQUID in a magnetometer configuration with a field-to-flux transfer coefficient of 35 nT/Φ_0; its flux noise was about 1.5 $\mu\Phi_0/\sqrt{Hz}$, and the field sensitivity was about 50 fT/$\sqrt{Hz}$. Much higher field sensitivities are possible of course, but since the thermal noise of the (room temperature) sample limits the useful sensitivity, it is wiser to make the inductance of the SQUID relatively small to achieve a low flux noise. A low inductance in turn leads to a relatively small effective area of the SQUID, which increases the dynamic range and thus the slew rate of the system. Because of the high excitation frequency of > 10 kHz and using lock-in detection, the system could be operated unshielded. With this system, Welzel *et al.* were able to detect all relevant defects in high-purity niobium sheets in an acceptable time with a high signal-to-noise ratio.

Fig. 7, left, shows a typical example of an eddy-current scan of such a sheet using a SQUID. A typical value for the change in the eddy current field induced by a 100-μm diameter Ta inclusion in a depth of 0.5 mm was about 30 pT. Although it seems possible to detect this field with a conventional magnetic field sensor, such as a flux gate, the then intolerably long measuring time would make the use of such a sensor impractical. For example, a flux gate with a rms field noise of 10 pT/$\sqrt{Hz}$ could detect a Ta inclusion with a signal-to-noise ratio SNR $\approx$ 1 in an integration time of 1 s. Assuming the area covered by the flux gate is 1 mm^2, it would take 300 × 300 s to scan a 30 × 30 cm^2 wide niobium sheet. Not only is this measuring time intolerably long, also an SNR $\approx$ 1 is insufficient to discriminate between noise and real defects. The desired SNR for relevant defects is > 30.

A drawback of eddy-current testing is the so-called 'lift-off effect'. Here, a variation in the stand-off distance between excitation coil and sample leads to a change in the eddy current density in the sample, and thus to a change in the eddy current field detected by the SQUID. Already small variations in the stand-off distance of the order of 10 μm produce field changes larger than the response from a Ta inclusion in the example described above. Pressing the excitation coil firmly onto the sample during scanning can reduce the lift-off effect caused by roughness of the sample. Nevertheless, when scanning the surface of the sample using a high excitation frequency (100 kHz), the lift-off effect is still noticeable. Spatial high-pass filtering [36] can reduce artefacts caused by the lift-off effect in this case.

To conclude, the above-described SQUID system was able to detect all relevant defects in niobium sheets with sufficient signal-to-noise ratio. Compared to a conventional system, the measured signal-to-noise ratio was better by a factor of up to 100, see also Fig. 7 (right). The scanning time of about 15 minutes required for a 30×30 cm^2 sheet was limited by the travel speed of the translation stage used; the high sensitivity of the system should allow for a shorter (say, 5 min.) scanning time without a noticeable loss in the signal-to-noise ratio.

Finally, Kreutzbruck *et al.* [37] performed eddy-current measurements with a HTS SQUID on aircraft parts to compare their SQUID NDE system with a commercial eddy-current NDE system (Elotest B1, Rohmann GmbH Frankenthal, Germany), which uses induction coils as field sensors. An induction coil without a ferrite core (PLA-44) was used in this test. The test sample was an aluminum plate with an artificial crack 40mm long, 0.15mm wide and 1.2mm deep, which was covered by another 13mm-thick aluminum plate. The crack was not detectable with the conventional system when a detection bandwidth of 30 Hz was used. Only in a bandwidth of 2 Hz could the crack be detected; the signal-to-noise ratio was still smaller than 3. With a HTS SQUID system, however, the crack could be detected with a signal-to-noise ratio of about 300 in a much larger bandwidth of 50 Hz.

Nondestructive evaluation using SQUID microscopes

The high spatial as well as the high field sensitivity make SQUID microscopes (see Chapter 9.3.5 by John Kirtley in this volume) ideal for nondestructive evaluation of certain types of materials, circuits or devices. For example, local defects, such as scratches and dents, as well as fatigue and mechanical stress can generate a remanent magnetization in certain stainless steels [38, 39]. This remanent magnetization can easily be detected with a SQUID [39, 40]. Gruhl *et al.* [41] examined the surface of several 1mm-thick stainless steel slabs with artificial scratches and dents. Figure 8 (upper right) shows a photograph of a stainless steel sample with various surface damages: six indentations caused by hammer strikes with various power, and several shallow scratches. The corresponding magnetic field distribution measured with a scanning SQUID microscope is shown in Fig. 8 (lower right). The stainless steel sample was not magnetized prior to the measurement, but was measured unshielded in the earth's magnetic field. It is found that the remanent magnetization is proportional to the strength of the mechanical stress: one can recognize the correlation between the strength with which the indentations were created and the magnetic field amplitude above the indentations. Although it is possible to measure such samples with conventional sensors by magnetizing the damaged stainless steel slabs, one will then lose the information about the force which with the defects were created. Similar finds were reported by Bonavolontà *et al.* [42].

SQUID microscopes have also been employed for the nondestructive evaluation of semiconducting circuits and photovoltaic cells. Several methods have been investigated to this end. Fleet *et al.* [43] tested microelectronic chips with a HTS SQUID microscope by measuring the magnetic field produced by electric current flowing in the circuits. They could identify shorts between pins of a packaged circuit and were able to locate the short to within ± 35 μm.

Dechert *et al.* [44] measured the current density in photovoltaic cells to detect internal shorts in their p-n-junction. An open-circuited photovoltaic cell was illuminated and the magnetic field above the cell was recorded. In the absence of internal shorts, no static magnetic field is produced by the cell. Detecting local fields enabled the authors to precisely locate shorts in the cell junction.

Beyer *et al.* [45] illuminated semiconducting wafers with a focused laser beam and measured the magnetic field of the net photocurrents induced in the sample with a niobium SQUID. They were able to detect changes in the doping of semiconducting wafers as well as electrically active defects, such as grain boundaries. They could also localize artefacts in photovoltaic devices. X.Y. Kong *et al.* [46] and Y. Nakatani *et al.* [47] performed similar measurements using high-temperature superconductor SQUIDs.

Gruhl *et al.* [41] also performed measurements on aircraft fuselage samples with their LTS SQUID microscope using the eddy current NDE method. They examined multilayer structures (up to four layers of aluminum sheet) of the fuselage of an Airbus A-300. The samples investigated with the SQUID microscope had a length of about 500 mm and had four rivet rows each containing 21 rivets. Figure 8 (bottom left) shows the cross section of the investigated samples, which consist of three layers of aluminum sheets. The top layer has a thickness of 1.4–2 mm, the second layer one of only 0.6–0.8 mm and the third layer is 1.8–2.5 mm thick. Due to cyclic stress loading, the defects usually occur in the third layer, and the fatigue cracks are most likely to develop along the direction of the fastener row. The titanium rivets had a diameter of 4.8 mm and a distance between each other of 22.5 mm. For eddy current measurements, a single wire positioned perpendicular to the rivet rows was used to excite eddy currents in the sample. The wire was positioned below the SQUID such that the excitation field was minimized at the location of the SQUID. No electronic compensation of the excitation field at the location of the SQUID was used. The excitation frequency was 2 kHz and the separation between sample and SQUID was 600 μm. Figure 8 (left) shows a line scan along a rivet row. In order to distinguish possible defect signals from signals caused by rivets, the magnetic field data were raised to the third power. Then the amplitudes of the signals generated by cracks are nearly proportional to the crack length. By exciting with a wire the signal of a flawless rivet shows an increase in magnetic field on one side of the rivet and a decrease on the other side. This is caused by induced currents, which flow in clockwise direction on one side and counter-clockwise on the other. A defect induces an additional current, which leads to an increase or decrease of the z-component of the magnetic field, depending on the position of the defect. It can be seen from Fig. 8 that the signals produced by the titanium rivets themselves are small compared to the signals due to cracks. Even a 1.2mm-long crack produces a signal, which is somewhat larger than the signal from a rivet without defect. Also shown in Fig. 8 (left) is a measurement of the same sample, using a SQUID inside a conventional cryostat. The stand-off distance between SQUID and sample here was about 6 mm. As the cracks to be detected are short, and as the distance between the rivets is relatively short as well, the high spatial resolution provided by the SQUID microscope is quite helpful when distinguishing possible defects from the signals generated by the rivets.

Conclusion

A large number of groups investigated the applicability of SQUIDs for nondestructive evaluation of a great variety of materials, ranging from food to aircrafts. A common find is that especially for the case of thick, highly conductive, or ferromagnetic materials, as well as sintered materials, the SQUID based systems show a much higher sensitivity compared to conventional eddy current, x-ray, or ultrasonic testing. The higher sensitivity and the larger dynamic range of the SQUID as compared to that of coils, magneto-resistive sensors or flux-gates, does improve the probability of finding a defect, and, more importantly, offers a substantial increase in testing speed. We note that a factor of only 2 in increased testing speed is already commercially very desirable, and justifies the use of a SQUID.

References

[1] R.J.P. Bain, G.B. Donaldson, S. Evanson, and G. Hayward, SQUID gradiometric detection of defects in ferromagnetic structures, in H.D. Hahlbohm and H. Lübbig (eds.), SQUID '85, (de Gruyter, Berlin 1985), pp. 841-846.

[2] S. Evanson, R.J.P. Bain, G.B. Donaldson, G. Stirling, and G. Hayward, "A comparison of the performance of planar and conventional second-order gradiometers coupled to a SQUID for the NDT of steel plates", IEEE Trans. Mag. **MAG-25**, 1200-1203 (1989).

[3] H. Weinstock, T. Erber, and M. Nisenoff, Threshold of Barkhausen emission and onset of hysteresis in iron, Phys. Rev. **B31**, 1535-1553 (1985).

[4] H. Weinstock and M. Nisenoff, Nondestructive evaluation of metallic structures using a SQUID gradiometer, in H.D. Hahlbohm and H. Lübbig (eds.), SQUID '85, (de Gruyter, Berlin 1985), pp. 853-858.

[5] T.E. Capobianco, J.C. Moulder, and F.R. Fickett, "Flaw detection with a magnetic field gradiometer", in D.W. Moore and G.A. Matzkan (eds.), *Proc. 15th Symposium on NDE*, NDE Testing Information Analysis Center, San Antonio, p. 15 (1986).

[6] J.G. Bellingham, M.L.A. Macvicar, and M. Nisenoff, "SQUID technology applied to the study of electrochemical corrosion", IEEE Trans. Mag. **23**, 477-479 (1987).

[7] A.D. Hibbs, R. Chung, and J.S. Pence, "Corrosion current measurement with a high resolution scanning magnetometer", in D.O.Thomson and D.E.Chimenti (eds.) Review of progress in quantitative NDE, Vol. **13A**, Plenum Press, New York, pp. 1955-1962 (1993).

[8] S. Wunderlich, F. Schmidl, H. Specht, L. Dörrer, H. Schneidewind, U. Hübner, and P. Seidel, "Planar gradiometers with high- DC SQUIDs for non-destructive testing", Supercond. Sci. Technol. **11**, 315-321 (1998).

[9] H. Weinstock, N. Tralshwala, and J.R. Claycomb, "Nondestructive evaluation of wires using high-temperature SQUIDs", IEEE Trans.Appl.Supercond. **AS-9**, 3797-3800 (1999).

[10] J.P. Wikswo, "SQUID magnetometers for biomagnetism and nondestructive testing: important questions and initial answers", IEEE Trans. Appl. Supercond. **5**, 74-120 (1995).

[11] R. Hohmann, M. Maus, M. Lomparski, M. Grüneklee, Y. Zhang, H.-J. Krause, H. Bousack, and A.I. Braginski, "Aircraft wheel testing with machine-cooled HTS SQUID gradiometer system", IEEE Trans. Appl. Supercond. **9**, 3801-3804 (1999).

[12] M. v. Kreutzbruck, U. Baby, A. Theiss, M. Mück, and C. Heiden, "Inspection of aircraft parts with high remanent magnetization by eddy current SQUID NDE", IEEE Trans.Appl.Supercond. **9**, 3805-3808 (1999).

[13] A. Ruosi, G. Pepe, G. Peluso, M. Valentino, and V. Monebhurrun, "Experimental and numerical results of electromagnetic nondestructive testing with HTc SQUIDs", IEEE Trans.Appl.Supercond. **AS-9**, 3499-3502 (1999).

[14] Y. Tavrin, M. Siegel, and J. Hinken, „ Standard method for detection of magnetic defects in aircraft engine discs using a HTS SQUID gradiometer ", IEEE Trans. Appl. Supercond. **AS-9**, 3809-3812 (1999).

[15] H.-J. Krause, W. Wolf, W. Glaas, E. Zimmermann, M.I. Faley, G. Sawade, R. Mattheus, G. Neudert, U. Gampe, and J. Krieger, "SQUID array for magnetic inspection of prestressed concrete bridges", Physica C **368**, 91-95 (2002).

[16] The SQUID Handbook Vol. II, eds. J.Clarke and A.I.Braginski, Wiley-VCH (Weinheim 2006).

[17] I.M.Thomas, Y.M.Ma, and J.P.Wikswo, 'Spatial resolution and sensitivity of magnetic susceptibility imaging', IEEE Trans.Appl.Supercond. **AS-3**, 1937-1940 (1993).

[18] C. Bonavolontà, M. Valentino, G. Peluso, F. Penta, A. Di Iorio, "Detection of mechanical fatigue in structural steel using SQUID and flux-gate sensors", Journal of Superconductivity and novel magnetism **22**, 833-839 (2009).
[19] T. Nagaishi, H. Ota, K. Nishi, K. Kuwa, T. Fujita, and S. Tanaka, "First Practical High Tc SQUID System for the Detection of Magnetic Foreign Substances in Commercial Products", IEEE Trans.Appl.Supercond. **AS-17**, 800-803 (2007).
[20] S. Tanaka, H. Fujita, Y. Hatsukade, T. Nagaishi, K. Nishi, H. Ota, T. Otani and S. Suzuki, "A food contaminant detection system based on high-Tc SQUIDs", Supercond. Sci. Technol. **19**, S280-S283 (2006).
[21] H. J. Krause, G. I. Panaitov, N. Wolters, D. Lomparski, W. Zander, Y. Zhang, E. Oberdoerffer, D. Wollersheim, W. Wilke, "Detection of Magnetic Contaminations in Industrial Products Using HTS SQUIDs", IEEE Trans. Appl. Supercond. **15**, 729-732 (2005).
[22] M. Bick, P. Sullivan, D. L. Tilbrook, J. Du, S. Gnanarajan, K.E. Leslie, and C.P. Foley , "A SQUID-based metal detector: comparison to coil and X-ray systems", Supercond. Sci. Technol. **18**, 346-351 (2005).
[23] S. Tanaka, H. Fujita, Y. Hatsukade, T. Otani, S. Suzuki, and T. Nagaishi, "A High Tc SQUID Micro-detector with a high performance magnetic shield for industrial products", Supercond. Sci. Technol. **20**, S385-S388 (2007).
[24] S. Tanaka, T. Akai, Y. Hatsukade, T. Ohtani, Y. Ikeda, S. Suzuki, K. Tanabe, "High Tc SQUID Detection System for Metallic Contaminant in Lithium Ion Battery", IEEE Trans. Magn. **45**, 4510-4513 (2009).
[25] *100 years of Superconductivity* (CRC Press Taylor & Francis Group, NW. (H. Rogalla and P.H. Kes, eds., 2011), p348.
[26] S. Tanaka, T. Akai, Y. Kitamura, Y. Hatsukade, T. Otani, and S. Suzuki, "Two-Channel HTS SQUID Gradiometer System for Detection of Metallic Contaminants in Lithium-Ion Battery", IEEE Trans. Appl. Supercond. **AS-21**, 424-427 (2011).
[27] A. Ghorbanpoor, "Magnetic-based NDE of steel in prestressed and post-tensioned concrete bridges". In R.D. Medlock and D.C. Laffrey (eds.), *Proc. Structural Materials Technology III*, SPIE Vol. 3400, San Antonio, TX, pp. 343-347 (1998).
[28] G. Sawade and H.-J. Krause, "Magnetic and electromagnetic non-destructive techniques for post-tensioning", in: COST 534, New Materials, Systems, Methods and Concepts for Prestressed Concrete Structures, Eds.: R.B. Polder *et al.*, COST Office, TNO Delft, pp. 209-240 (2010).
[29] G. Sawade and H.-J. Krause, „Prüfung von Spannbetonbauteilen mit magnetischen Methoden", Beton- und Stahlbetonbau **105**, 154-164 (2010).
[30] G. Sawade, H.-J. Krause, and U. Gampe, in M. T. Forde (ed.) *Proceedings of the 7th international conference on Structural Faults and Repair – 97*, Vol. I, Engineering Technical Press, Edinburgh 1997, pp. 401-406.
[31] M.I. Faley, U. Poppe, K. Urban, E. Zimmermann, W. Glaas, H. Halling, M. Bick, H.-J. Krause, D.N. Paulson, T. Starr, and R.L. Fagaly, "Operation of the HTS dc-SQUID Sensors in High Magnetic Fields", IEEE Trans.Appl.Supercond. **AS-9**, 3386-3391 (1999).
[32] A. Ruosi, M. Valentino, V. Lopresto, and G. Caprino, Magnetic response of damaged carbon fibre reinforced plastics measured by a HTS-SQUID magnetometer, Composite Structures **56**, 141–149 (2002).
[33] D. Graham, P. Maas, G.B Donaldson, and C. Carr, Impact damage detection in carbon fibre composites using HTS SQUIDs and neural networks, NDT & E International **37**, 565–570 (2004).

[34] C. Bonavolontà, G. Peluso, G.P. Pepe, M. Valentino, "Detection of Early Stage Damage In Carbon Fiber Reinforced Polymers For Aeronautical Applications Using An HTS SQUID Magnetometer", Eur. Phys. J. **B 42**, 491-496 (2004).
[35] C. Bonavolontà, M. Valentino and G.P. Pepe, "Characterization of the damage process in GLARE® 2 using an eddy current technique based on HTS-SQUID magnetometer", Supercond. Sci. Technol. **20**, 51-56 (2007).
[36] C. Welzel, PhD Thesis, University of Giessen (2003). M. Mück, C. Welzel, A. Farr, F. Schölz and W. Singer, IEEE Trans.Appl.Supercond. **AS-13,** 239-244 (2003).
[37] M. v. Kreutzbruck, U. Baby, M. Mück, and C. Heiden, "Experiments on eddy current NDE with HTS rf SQUIDs", in *Studies in Applied Electromagnetics and Mechanics*, Vol. **15**, IOS, Amsterdam, pp. 457–463 (1998).
[38] A. Seeger, H. Kronmüller, H. Rieger, and H. Träuble, „Effect of Lattice Defects on the Magnetization Curve of Ferromagnets", J. Appl. Phys. **35**, 740-742 (1964).
[39] T.J. Shaw, K. Schlenga, R. McDermott, J. Clarke, J.W. Chan, S.-H. Kang, and J.W. Morris, "High-T_c SQUID microscope study of the effects of microstructure and deformation on the remanent magnetization of steel", IEEE Trans. Appl. Supercond. **9**, 4107-4110 (1999).
[40] N. Kasai, N. Ishikawa, H. Yamakawa, K. Chinone, S. Nakayama, and A. Odawara, "Nondestructive detection of dislocations in steel using a SQUID gradiometer", IEEE Trans. Appl. Supercond. **7**, 2315-2318 (1997).
[41] F. Gruhl, M. Mück, M. v. Kreutzbruck and J. Dechert, "A scanning superconducting quantum interference device microscope with high spatial resolution for room temperature samples", Rev. Sci. Instrum. **72**, 2090-2096 (2001).
[42] C. Bonavolontà, M. Valentino, M. Adamo, E. Sarnelli, "Detection of plastic deformation in structural steel using scanning SQUID microscopy", Meas. Sci. Technol. **18**, 2116-2120 (2007).
[43] E.F. Fleet, S. Chatraphorn, F.C. Wellstood, and L.A. Knauss, "HTS scanning SQUID microscopy of active circuits", IEEE Trans. Appl. Supercond. **AS-9**, 4103-4106 (1999).
[44] J. Dechert, Hochauflösende Raster-SQUID Mikroskopie, Dissertation, University of Giessen, (1999). J. Dechert, M. Mück, and C. Heiden, "A scanning SQUID microscope for samples at room temperature", IEEE Trans.Appl.Supercond. **AS-9**, 4111-4114 (1999).
[45] J. Beyer, D. Drung, and T. Schurig, "SQUID photoscanning: an imaging technique for NDE of semiconductor wafers and devices based on photomagnetic detection", IEEE Trans.Appl.Supercond. **AS-11**, 1162-1167 (2001).
[46] X.Y. Kong, K. Kojima, K. Sakuta, H. Itozaki, Current vector distribution in semiconductor observed by laser SQUID microscope with needle, Physica **C 463-465**, 1048-1051 (2007).
[47] Y. Nakatani, T. Hayashi, and H. Itozaki, "Observation of Polycrystalline Solar Cell Using a Laser-SQUID Microscope", IEEE Trans. Appl. Supercond. **21**, 416-419 (2011).

Figure Captions

Fig.1. Basic principle of nondestructive evaluation of ferromagnetic plates using a magnetic field sensor, such as a SQUID (see text).

Fig. 2. Principle for detection of contaminants in metallic sheets.

Fig. 3. Left: Change in magnetic field produced by small metallic balls, and right: Magnetic flux produced by these balls at the SQUID as a function of ball diameter.

Fig. 4. Principle of magnetic detection of ruptures in tendon strands of prestressed concrete beams.

Fig. 5. Rupture signal amplitudes measured with the stray field and the remanent field technique on the bridge [29]. The circle marks an indication above threshold.

Fig. 6. Basic principle of eddy current NDE (left), and measurement configuration used to test niobium sheets with a SQUID (right).

Fig. 7. Left: Two-dimensional distribution of the eddy current field above a 22 cm by 22 cm size niobium sheet. The excitation field generated by a 3-mm diameter coil was about 0.6 mT peak-to-peak; the eddy-current frequency was 10 kHz, measurement time was about 15 minutes. Ta inclusions (bright spots) are clearly detected. Right: Same sheet measured with conventional eddy-current NDE system. Most defects are obscured by noise.; scanning time and measurement bandwidth same as for SQUID measurement.

Fig. 8. Nondestructive evaluation using a scanning SQUID microscope. Left: eddy current test of a wing section of an Airbus A-300 showing eddy current field measured with SQUID microscope (solid line) and SQUID in conventional cryostat (dashed line). Cross section of sample consisting of three aluminum layers with rivets (gray vertical bars) and cracks adjacent to rivets (black boxes in lowest aluminum layer) is shown below. Right: optical image (upper) and magnetic image (lower picture) of stainless steel slap with three indentations (scanned area is 5×5 mm^2).

Fig.1

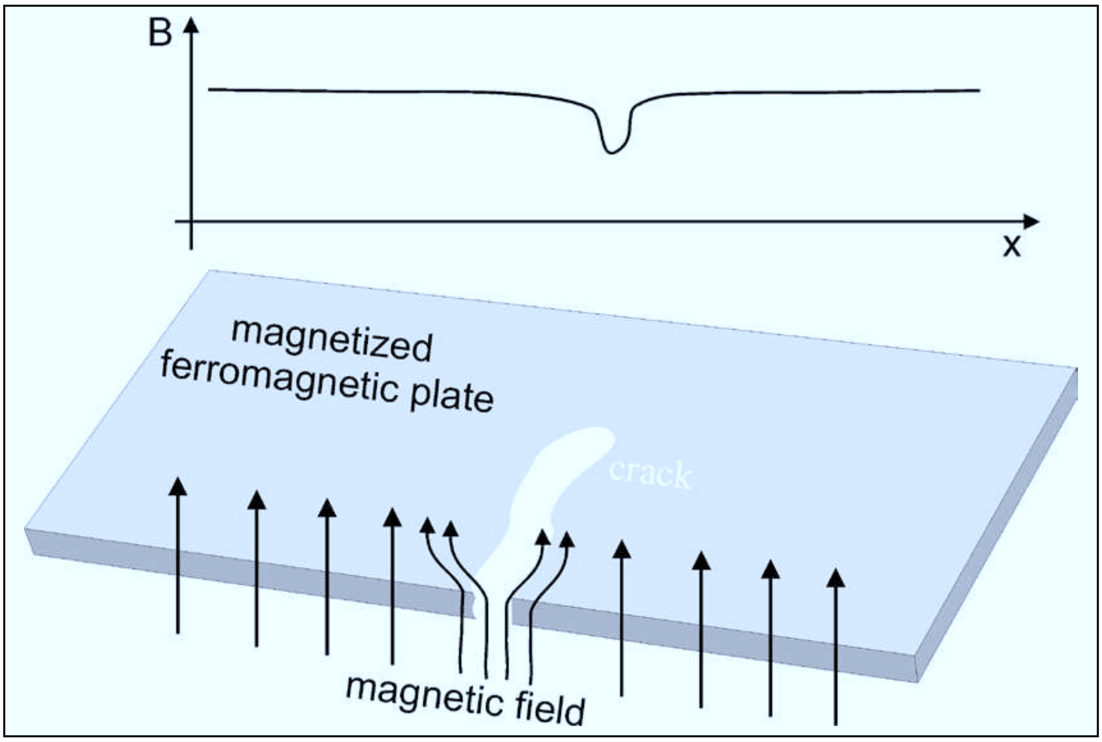

Fig. 2

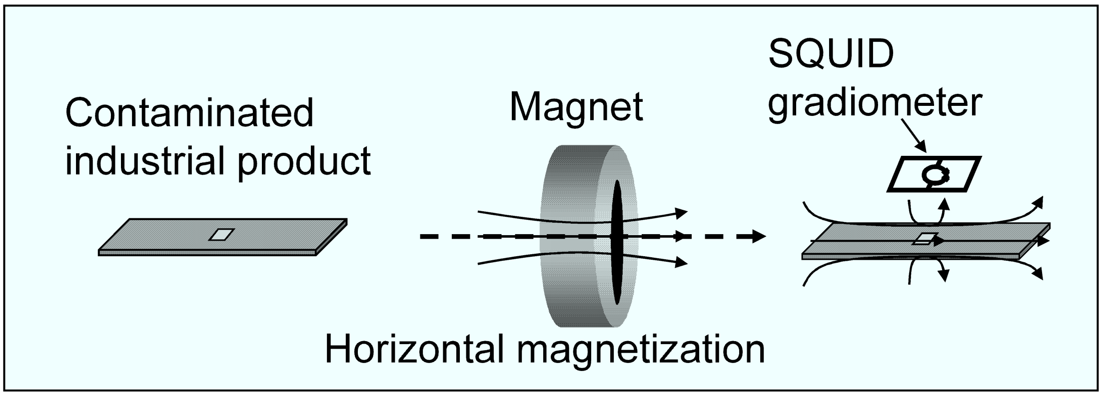

Contaminated
industrial product
Magnet
SQUID
gradiometer
Horizontal magnetization

Fig. 3

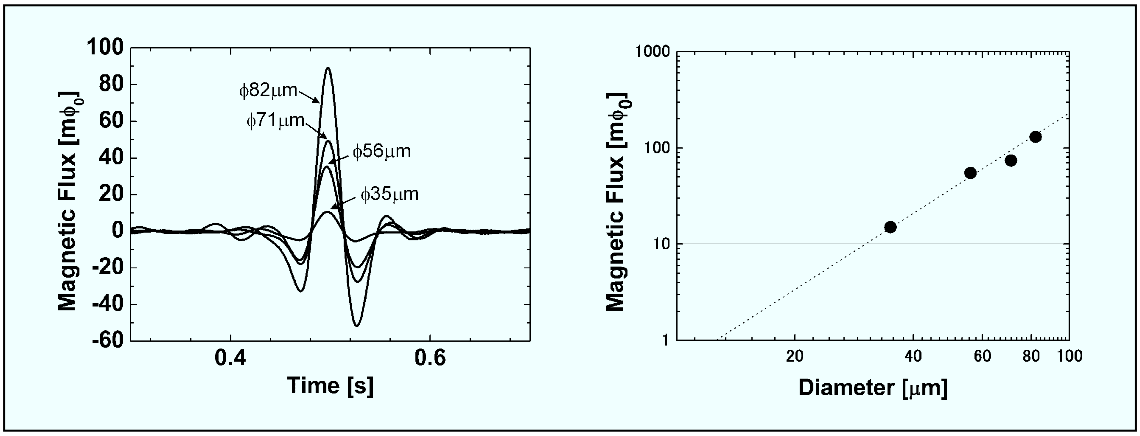

Magnetic Flux [mϕ0]
Time [s]
ϕ82μm
ϕ71μm
ϕ56μm
ϕ35μm
Magnetic Flux [mϕ0]
Diameter [μm]

Fig. 4

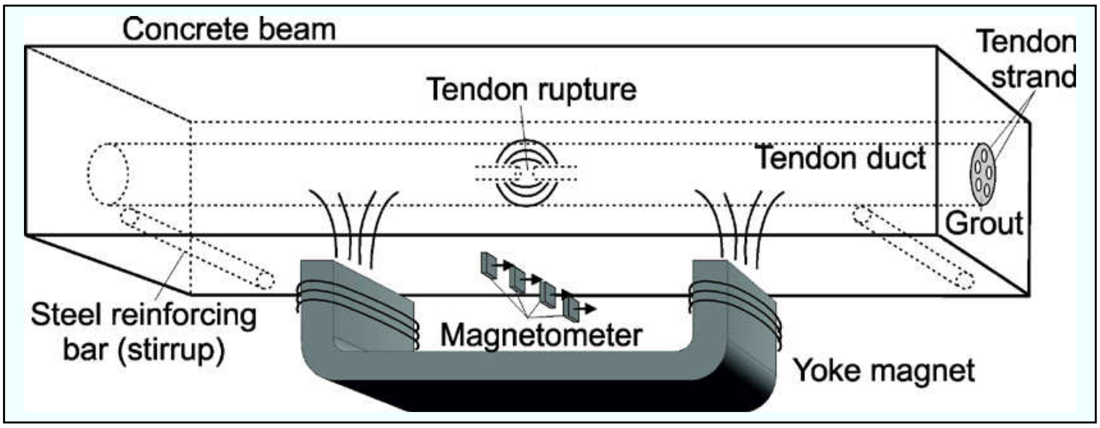
Concrete beam
Tendon rupture
Tendon strand
Tendon duct
Grout
Steel reinforcing
bar (stirrup)
Magnetometer
Yoke magnet

Fig. 5

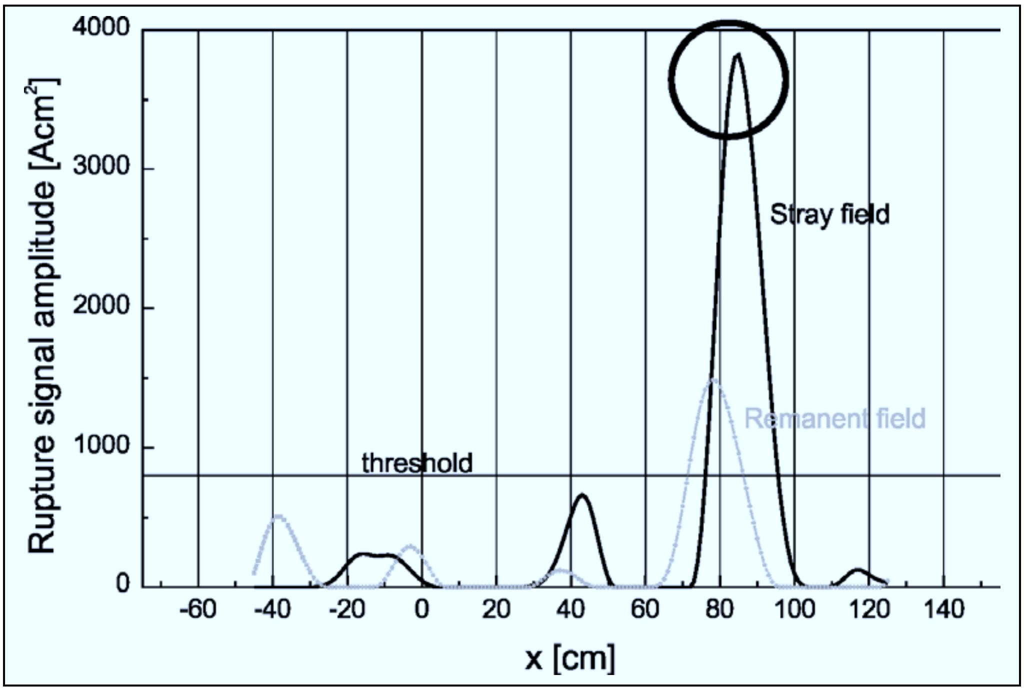

Rupture signal amplitude [Acm^2]
4000
3000
2000
1000
0
Stray field
Remanent field
threshold
-60
-40
-20
0
20
40
60
80
100
120
140
x [cm]

Fig. 6

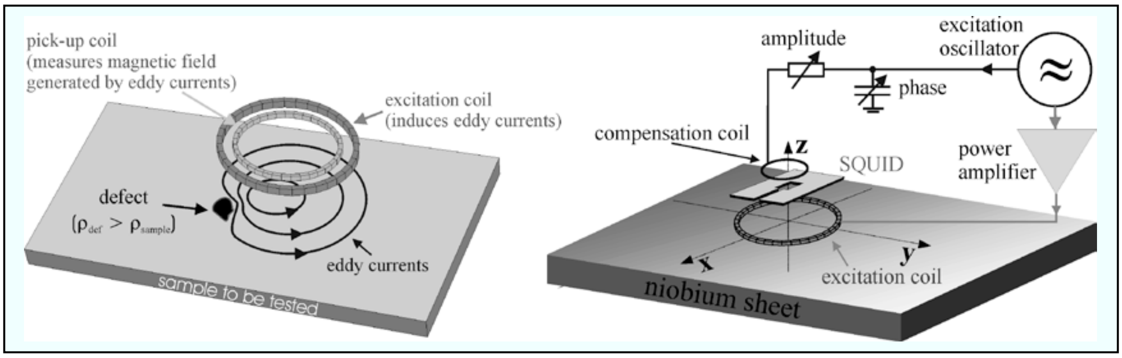
pick-up coil
(measures magnetic field
generated by eddy currents)
excitation coil
(induces eddy currents)
defect
($\rho_{def} > \rho_{sample}$)
eddy currents
sample to be tested
amplitude
excitation
oscillator
phase
compensation coil
z
SQUID
power
amplifier
x
y
excitation coil
niobium sheet

Fig. 7

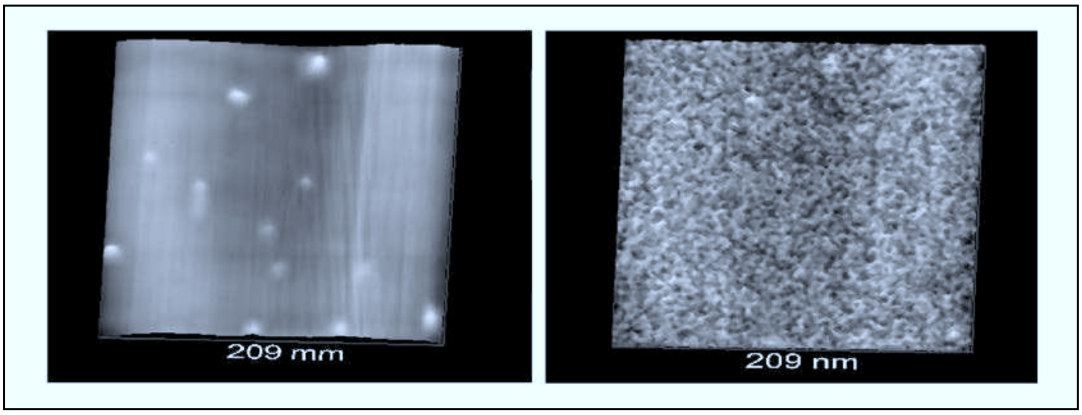

Fig. 8

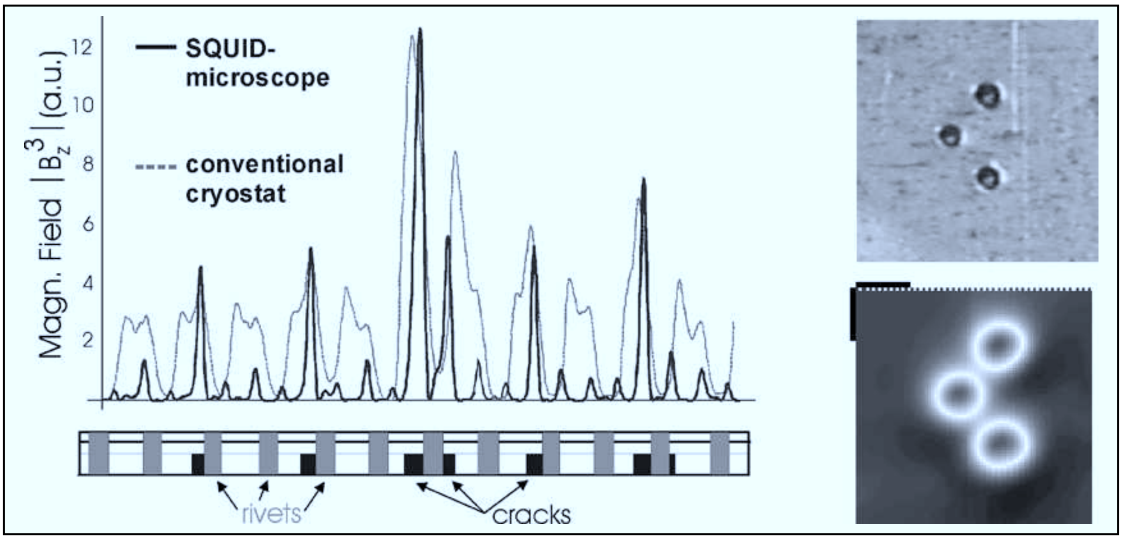

SQUID-microscope
conventional cryostat
Magn. Field $|B_z^3|$ (a.u.)
12
10
8
6
4
2
rivets
cracks